Wear 450-451 (2020) 203272

Contents lists available at ScienceDirect

Wear

journal homepage: http://www.elsevier.com/locate/wear

Hydraulic convey of iron ore slurry: Pipeline wear and ore particle degradation in function of pumping time

José Wilmar Calderón-Hernández [a,e,*], Amilton Sinatora [b,e], Hercílio G. de Melo [a], Arthur P. Chaves [c], Eliana S. Mano [c], Laurindo S. Leal Filho [c], José L. Paiva [d], André S. Braga [c], Thiago C. Souza Pinto [e]

[a] Escola Politécnica da Universidade de São Paulo, Departamento de Eng. Metalúrgica e de Materiais, Av. Prof. Mello Moraes, 2463, 05508-030, São Paulo, SP, Brazil
[b] Escola Politécnica da Universidade de São Paulo, Departamento de Eng. Mecânica, Av. Prof. Mello Moraes 2231, 05508-030, São Paulo, SP, Brazil
[c] Escola Politécnica da Universidade de São Paulo, Departamento de Eng. de Minas e de Petróleo, Av. Prof. Mello Moraes 2373, 05508-030, São Paulo, SP, Brazil
[d] Escola Politécnica da Universidade de São Paulo, Departamento de Eng. Química, Av. Prof. Lineu Prestes, 580 - 05508-000, São Paulo, SP, Brazil
[e] Instituto Tecnológico Vale, Av. Juscelino Kubitschek 31, Bauxita, Ouro Preto, MG 35400-000, Brazil

ARTICLE INFO

Keywords:
Iron ore slurry
Pipeline wear
Erosion-corrosion
Synergism

ABSTRACT

This paper reports and discusses the results of an experimental investigation on hydraulic transportation of iron ore concentrate and its effect on slurry wear, pure erosion and pure corrosion of a carbon steel pipe. For this, a specially designed test-loop was built to simulate long distance iron ore transportation, allowing also to determine pure erosion effects by means of a specially designed cathodic protection system. Pure corrosion damage was evaluated by linear polarization measurements in filtered ore concentrate, *i.e.,* in the absence of particles. The results revealed that pure erosion and pure corrosion effects were much lower than the measured wear, evaluated as pipe thickness loss, indicating an important synergism between erosion and corrosion. Wear damage results in microcraters aligned in the flow direction, which merge with each other likely due to enhanced electrochemical activity fed by the erosion process. Evaluation of the effect of the pumping time on the ore concentrate characteristics revealed that particles sizes decreased while the sphericity factor increased leading to lower wear rates. Finally, a mechanism explaining the pipeline wear associating erosion, corrosion and the material microstructure as well as a methodology to forecast the pipelines thickness loss as a function of the ore concentrate travelling distance were also proposed.

1. Introduction

Brazil is known worldwide as one of the main global suppliers of iron ore concentrates [1,2]. In 2017, Brazil produced more than 440 million tons of final concentrates, mainly as sinter and pellet feed. This large production capacity requires a complex transport network, mainly comprising railroad, maritime and pipelines. The hydraulic transportation of solids through pipelines has been widely used as an effective and cost-saving method [3]. Regarding the medium-long network pipelines, Brazil currently presents around 915 km in operation for iron ore pellet feed products [4].

Wear is a serious problem in the mining industry. Slurry pipelines operate at relatively high pressure to move the pulp, and undesirable leaks can eject tons of material in a short period of time causing environmental and economic losses [5–7]. Regarding the hydraulic conveyance of iron ore pellet feed concentrate slurry, the pipeline system must be designed to resist physical and chemical alterations caused by the interaction of mineral particles with the pipeline surface, erosion, corrosion as well as the combination of all of them. The slurry characteristics, such as mineralogical composition, hardness, size and shape of particles result in different wear rates on the pipe wall. Actually, the mineralogical aspects of the iron ore concentrates should be considered; high erosion rates are attributed to alumina and quartz; conversely, limestone and red mud are considered to be less aggressive [8].

Since the 1980s, industrial countries have estimated losses of about 0.3%–3.0% of their gross domestic product (GDP) with wear problems [9]. The National Council of Canada [10] reported that in 1982, the country lost around 940 million dollars in the mining industry due to wear issues. Recent data estimate that friction and wear in mineral mining result in annual economic losses of about 210,000 million Euros,

* Corresponding author.
E-mail address: wilmar.calderon.hernadez@usp.br (J.W. Calderón-Hernández).

https://doi.org/10.1016/j.wear.2020.203272
Received 15 November 2019; Received in revised form 24 February 2020; Accepted 16 March 2020
Available online 23 March 2020

distributed as follows: 40% for overcoming friction, 27% for producing replacement parts and spare equipment, 26% for maintenance work and 7% for lost production [11]. Therefore, in recent years, researchers have invested time and resources investigating the mechanisms of wear associated with erosion-corrosion aiming to develop new corrosion inhibitors and materials offering higher resistance to damages caused by mining operations. Consequently, different experimental devices, such as slurry pot erosion tester [12–20], jet impingement rings [21–27], Coriolis erosion tester [28–30], rotating cylinder apparatus [31–34], and some pipeline scale flow-loop [35–39] have been designed to create a better understanding of total wear, and the synergism of erosion/corrosion in pipelines. Clearly, the results show that erosion and corrosion interact synergistically, producing wear rates significantly higher than the simple sum of both effects.

Investigations about the wear rate in function of slurry aging are not common, especially with fine ore particles in recirculation scale loops, but the general literature highlights the importance of particle degradation in determining wear rates [40,41]. However, laboratory conventional setups [12–34] are far from representing real ore slurry transportation, where interactions take place along several kilometers of pipelines and the slurry particles are constantly being modified. For instance, in the SAIT2000 conference in South Africa a laboratory apparatus for evaluating slurry pipeline wear was presented [42], the authors compared the wear rates obtained with the apparatus (approximately 0.60 mm/year) with actual wear rates at the bottom of 550 mm diameter operating pipelines conveying the fine tailings (between 0.88 and 1.23 mm/year) concluding that regarding the effect of particle properties (size, shape, hardness, etc), conveying velocity and solids concentration on wear rate cannot be made unless a correction is made for the changes in slurry wear.

Normally, mining industries do not reveal detailed information about maintenance and failure analysis on their pipelines. On the other hand, the use of pilot scale loops in research institutes is not common due to the expensive infrastructure, the considerable size of the loops and the need of technical people support. Therefore, there is a lack of published information about wear damages on real iron ore slurry transportation situations. In order to contribute towards a better understanding of the slurry wear mechanism caused by the iron ore pellet feed slurry in hydraulic transportation, in the present work a pilot scale flow-loop with a particular device allowing to separate pure erosion contribution from the total wear damage was designed. The work is focused in evaluating the effects of flow rate as well as on the evaluation of the effects of ore slurry aging (travelling distance) on wear damages. Individual contributions of corrosion and erosion to the pipeline were estimated and their synergistic effects discussed in the light of the results of the obtained wear damages.

2. Materials and methods

2.1. Pipeline test loop

The experiments were conducted with a fixed concentration of solids (by weight) and two flow velocities. The first one was set slightly higher than the critical velocity (Vc - graphically determined as shown in section 3.4) and the second was set close to twice Vc.

A 35-m long pilot-scale test loop facility (Fig. 1) comprising two different pipe diameters ($D_1 = 100$ mm and $D_2 = 75$ mm) and a lined rubber centrifugal pump of 30 kW was used. The results of total wear and its mechanisms (pure erosion and erosion/corrosion synergisms) were evaluated at the pipe with the largest diameter (D_1), as the bigger the diameter, the higher the load of bed particles flowing at the pipe bottom.

Two 1-m-long pipe sections were installed between flanges for assessing the wear (indicated by arrows in Fig. 1). A sample holder was developed to be placed inside of these pipe sections, allowing evaluating separately the total wear and the effects of pure erosion (details in section 2.2).

The experimental procedure was conducted firstly by setting the slurry concentration in the feed tank to 60% solids by weight. The pump was then set in motion progressively, increasing its velocity up to the full movement of the slurry inside the pipes. A special section made of transparent Perspex was employed for visually observing the settling

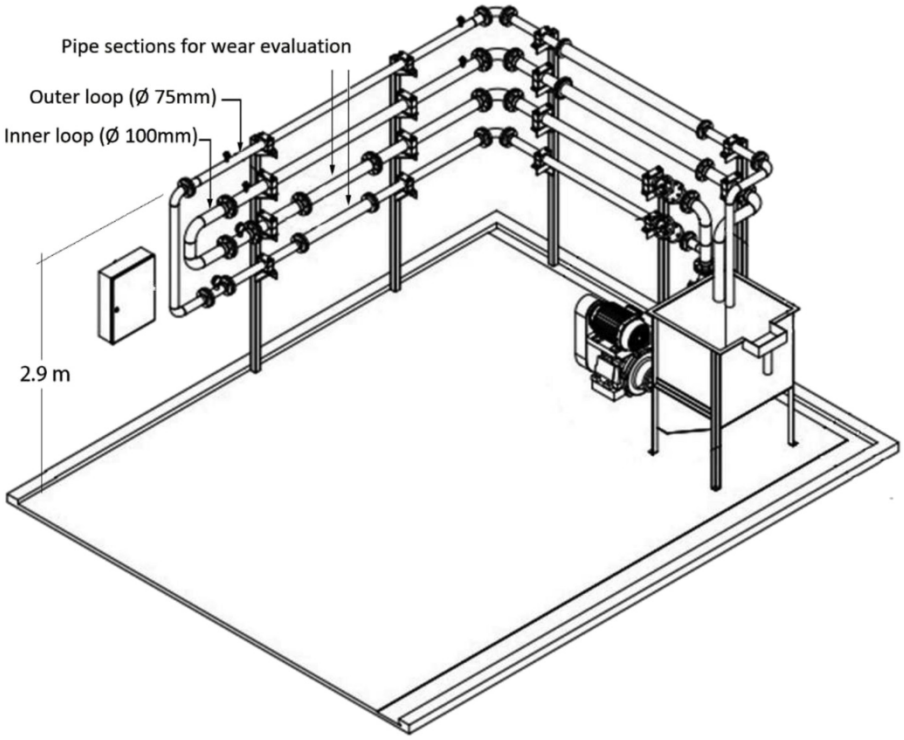

Fig. 1. Schematic of pipeline test loop - Inner loop of 100 mm dimeter and outer loop of 75 mm diameter.

behavior of particles inside the pipes. Once steady conditions were achieved, the gathering of data started. A frequency inverter controller was used to vary the pump as well as the flow velocity, and a full range of magnitude was covered. The critical velocity (Vc) was estimated by plotting the flow velocity versus pressure drop per horizontal meter of pipe, as will be described later.

2.2. Wear test apparatus

These tests were carried out in a specially designed system allowing to evaluate the slurry wear without introducing any flow disturbance. For this, concave test coupons (27 cm^2 of exposed area) were cut from a steel pipeline piece and machined to exactly fit to a specimen holder as shown in Fig. 2(b). The ensemble was then positioned to contact the iron ore slurry at the bottom of the 100 mm diameter flanged pipes in the pilot-scale test loop facility (Fig. 2(c)).

The coupons were made of a commercial steel pipe ASTM A106 B (nominal composition shown in Table 1), previously sanded with 1200 grit SiC emery paper. The specimen holder was also made of a steel ring extracted from a piece of pipe.

After the test completion, the coupon was taken out from the holder to evaluate the wear morphology and the intensity of the corrosive attack by the weight loss method. The main advantage of the designed system is that a real procedure of pumping of mineral slurries can be simulated. Indeed, other systems used for wear evaluations as jet impingement or slurry pot erosion rigs do not reproduce the hydrodynamic forces and the rheological characteristics inside the pipeline during pumping. The first variable defines the angle and impact force of particles and the second the viscosity, both variables strongly affect the pipeline wear. For instance, jet impingement rigs are used to study the angle and intensity impact of particles which can be adequate to qualify the erosion resistance between materials but is not adequate to determine the wear rate in real systems.

Aiming to assess the effect of the ore slurry aging on the wear rate and morphology, the test coupons were exposed for different periods to the circulating fluid after different pumping times, as described in Table 2 (the term aging refers the ore particles degradation induced by pumping time). To obtain the weight loss, the coupons were weighed before and after each test period in a digital balance with an accuracy of ±0.0001 g. Five measurements were taken. The wear rates were calculated as thickness loss (mm/year) using Eq. (1), wherein Δm is the average mass loss, 7.8 E^{-3} g/mm^3 is the steel density and 2700 mm^2 the exposed area (27 cm^2).

$$Erosion\ rate\ (mm/day) = \frac{\Delta m\ (g) \times 24 \times 365}{2700\ mm^2 \times 0.0078\ \frac{g}{mm^3} \times Time\ test\ (hours)} \quad (1)$$

Table 2 describes the experimental sequence for the weight loss experiments, which was divided in two sessions. In the first one, 1 ton of fresh slurry was prepared and pumped at 1.6 (m/s) and the weight loss measured every 8 h, for different coupons, until 40 h of pumping, therefore, each coupon (1a to 5a) was exposed for the same time interval to the slurry with different aging times (indicated in the last column). After that the loop was evacuated and washed and the second run started. For this latter run, another ton of fresh iron ore slurry was prepared, which was then pumped at 3 m/s. In this run the weight loss was measured for coupons exposed for different time intervals to slurry with different aging times, until 90 h of pumping. In Table 2, the second column shows the interval by which each coupon was exposed to the circulating slurry, whereas the last column describes the slurry aging time prior to the beginning of each experiment (coupons 1b–6b). For each weight loss measurement, the engine pump was turned off and the loop accessed to remove and replace the coupon, which was then reweighted to calculate the wear rate and some of them were examined to evaluate the wear morphology.

It is important to stress that this type of test has operational complexities, as it is a relatively robust pumping system, requires technical support personnel for operation and large amounts of pulp to simulate a real pumping system (one ton per session). As the iron ore slurry degrades with pumping time, the test is destructive. Iron ore extracted from a Brazilian mine 640 km from the research center was made available for this investigation. The received material was rigorously characterized and the amount was sufficient to prepare two tons of 60 wt

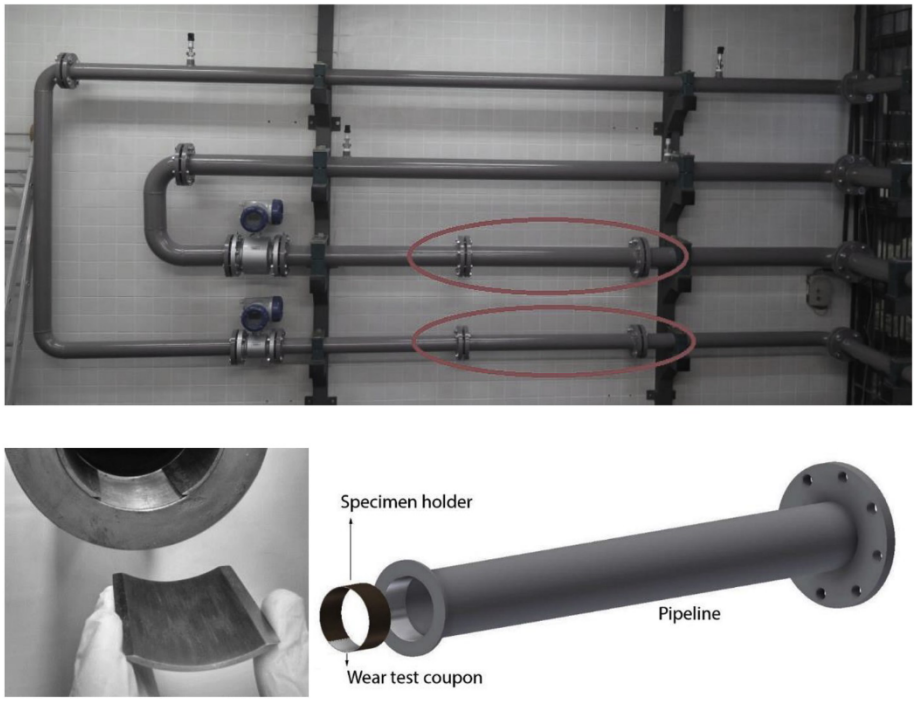

Fig. 2. (a) Photo of the pilot pilot-scale test loop facility indicating the two flanged pipe sections; (b) Concave test coupon machined to fit the sample holder; (c) Schematic representation of the mounted specimen holder prior to its introduction inside the pipeline.

Table 1
Nominal chemical composition of ASTM A106 B (wt%).

C (max)	Mn	P (max)	S (max)	Si (min)	Cr (max)	Cu (max)	Mo (max)	Ni (max)	V (max)
0.3	0.25 to 0.93	0.035	0.035	0.10	0.40	0.40	0.15	0.40	0.08

Table 2
Test conditions for erosion assessment.

Test	Time of coupon exposure to the circulating fluid (hours)	Slurry concentration and velocity	Pumping interval examined (accumulated hours)
	First pumping session - 40 h		
Coupon 1a	8	60 wt% - 1.6 m/s	Starting with fresh slurry.
Coupon 2a	8		Starting with slurry already pumped for 8 h.
Coupon 3a	8		Starting with slurry already pumped for 16 h.
Coupon 4a	8		Starting with slurry already pumped for 24 h.
Coupon 5a	8		Starting with slurry already pumped for 32 h.
	Second pumping session - 90 h		
Coupon 1b	3	60 wt% - 3 m/s	Starting with fresh slurry.
Coupon 2b	6		Starting with slurry already pumped for 3 h.
Coupon 3b	10		Starting with slurry already pumped for 20 h.
Coupon 4b	10		Starting with slurry already pumped for 60 h.
Coupon 5b	3		Starting with slurry already pumped for 75 h.
Coupon 6b	10		Starting with slurry already pumped for 80 h.

% concentrated pulp (one ton for each velocity studied, i.e., one ton for session).

2.3. Determination of pure corrosion (without erosion)

In order to obtain the corrosion rate individually, linear polarization resistance (LPR) measurements under static and turbulent conditions were performed using filtered water from the slurry as electrolyte. The former measurements were performed in a classical three-electrode electrochemical cell, whereas the latter tests used a setup specially designed to simulate turbulent environments inside a 5 L volume electrochemical corrosion cell; the turbulence was created by a polymeric disc coupled to a shaft rotating at 200 RPM [43]. In both cases, a scan velocity of 1 mV/s was employed and cubic pieces of steel (SiC sanded up to 1200 grit) embedded in bakelite with 1 cm^2 of exposed area were used as working electrodes, with a platinum wire as the counter electrode and a saturated calomel (SCE) as the reference electrode. The experiments were controlled by a potentiostat/galvanostat (PAR model 273A) and the thickness loss, in mm/year, was determined from the polarization resistance (Rp) values using the Stern-Geary equation and Faraday's law [44].

2.4. Determination of pure erosion (without the corrosion effect)

To evaluate pure erosion, *i.e.* the damage caused by the slurry without the influence of corrosion, a cathodic protection system was designed at which the steel coupon was galvanically coupled to a Zn piece (50 cm^2). To mount the galvanic cell, the zinc sheet was placed in the sample holder ring, from which it was electrically isolated by a rubber sheet as shown in Fig. 3(c). Afterwards, the Zn anode and the test coupon were externally connected by means of a set of screws and an external cable (Fig. 3(b)) and then exposed for 3 h to the iron ore slurry concentrated at 60 wt% at a flow rate of 1.6 m/s.

In this case 3 coupons were tested for 3 h (each one) with the slurry used for the first pumping session after the experiments designed in Table 2. Table 3 shows the conditions tested with cathodic protection.

After the completion of the experiments, the steel coupons were removed, washed with distilled water and ethanol, dried in a hot air stream and the exposed surface was analyzed with an optical microscope (Olympus BX60 M) and with and a noncontact surface profiler CCI MP using the softwares Talysurf and Talymap (Taylor Hobson).

2.5. Characterization of the iron ore sample

For the characterization procedures, slurry aliquots of 1.5 and 0.5 kg were withdrawn from the homogenized ore sample. Chemical analyses by X-ray fluorescence (XRF) and loss on ignition (LOI) were conducted with the 0.5 kg aliquot. The XRF analyses were carried out from the molten bulk sample with anhydrous lithium tetraborate. Loss on ignition (LOI) was determined from 1 g of the bulk sample, which was dried at 100 °C to evaporate water and then heated at 1020 °C for 2 h. Afterwards, it was placed in a desiccator to cool prior to be weighed.

Size distribution was determined by wet sieving in 0.297 mm, 0.21 mm, 0.15 mm, 0.1 mm, 0.074 mm and 0.037 mm sieves. The size fractions lower than 0.037 mm were classified by a cyclosizer (Sepor INC) in 30, 20, 10, 9, 6 and < 6 μm.

The ore minerals were identified by X-ray powder diffraction (XRD); the patterns were recorded on a Bruker D8 Endeavor diffractometer (Cu Kα radiation - 40 kV, 40 mA- Lynx eye detector) from 2 to 70° with steps of 0.02° and a counting time of 115 s per step (converted from the scanning mode). The software HighScore Plus was used to analyze the patterns. The ore mineralogy was estimated conjugating XRF and XRD results.

The shape factor of the iron ore concentrate was evaluated through the sphericity function (Ψ) and determined by the permeametry method [45] for the bulk concentrate and for the sample after 90-h pumping. To distinguish the iron and quartz particles, dried ore samples were mounted in bakelite, polished to 1 μm, coated with carbon and examined by SEM-EDX (Sprit Bruker coupled to a SEM Quanta 650 FEG of FEI).

2.6. Microstructural characterization of the steel coupons

To characterize the steel microstructure, a sample of 1 cm^2 was cut, embedded in bakelite, metallographically polished up to 1 μm and then etched by immersion in Nital 2% (2 ml HNO_3 + 98 ml ethyl alcohol). Afterwards, it was washed with ethyl alcohol and the microstructure examined by optical microscopy. The optical microscopy of polished samples was also employed to evaluate inclusions distribution.

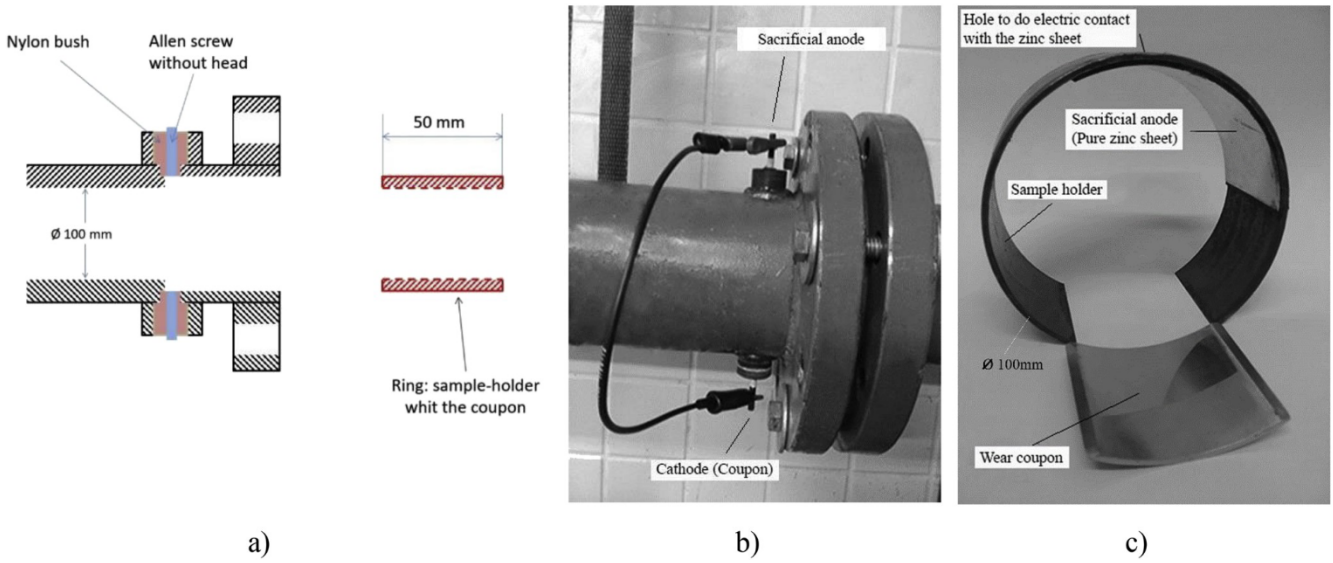

Fig. 3. Experimental arrangement for pure erosion evaluation. a) General sketch. b) External connection closing the electrical circuit. The coupon and zinc sheet were isolated from any electrical contact with the loop metallic material. c) Sample holder with a zinc sheet as sacrificial anode and the coupon.

Table 3
Conditions tested with cathodic protection.

Test	Time of coupon exposure to the circulating fluid (hours)	Slurry concentration and velocity	Pumping interval examined (accumulated hours)
Coupon 6a	3	60 wt% - 1.6 m/s **With cathodic protection**	Sequential tests done with the iron ore pumped previously for 40 h (Table 2 – First session)
Coupon 7a	3		
Coupon 8a	3		

3. Results

3.1. Iron ore characterization

According to the chemical analysis by XRF combined to XRD data from the bulk sample, (Table 4 and Fig. 4), the ore slurry is predominantly composed of Fe oxides and hydroxides (hematite and goethite, respectively). There is a small content of quartz: less than 3 wt%. XRF results (Table 4) for the different size fractions revealed that quartz is present especially in the coarsest fractions (297–149 μm). In turn, Fe oxides and hydroxides are especially present in the finest fractions (<149 μm).

The particles sizes distribution for the bulk sample and for the samples after 10, 22, 32, and 90 h pumping are shown in Fig. 4 (samples extracted from the iron ore slurry of the second pumping test – Table 2). It shows that more than 60% (wt%) of the bulk sample exhibited size

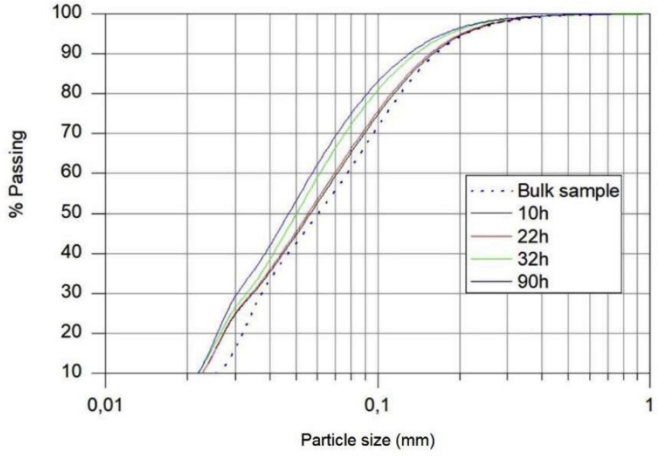

Fig. 4. Particle size distribution for bulk sample (0 h), and samples after 10-h, 22-h, 32-h and 90-h pumping.

fraction smaller than 0.08 mm (80 μm). It also evidences that size distribution changes with pumping time and that the particles sizes are progressively reduced. For instance, the bulk sample (0 h) exhibited a $P_{90} < 140$ μm, whereas the 90-h sample shows $P_{90} = 120$ μm and P_{60} lower than 60 μm (P_{90} and P_{60} means 90% and 60% passing - Fig. 4).

Concerning the shapes of the particles, the higher the pumping time, the higher their sphericity (Ψ), indicating that they tend to become more round-shaped as pumping time increases. The bulk concentrated

Table 4
XRF analysis from the bulk sample and sizing fractions products (wt%).

Size fraction (μm)	Al_2O_3	SiO_2	P_2O_5	SO_3	TiO_2	MnO	Fe_2O_3	LOI	%
bulk sample	0.99	2.69	0.15		0.1	0.1	92.2	3.5	
297	3.96	13.9	0.25	0.03	0.13	0.194	72.2	9.17	1.94
−297 + 210	2.67	13.2	0.225	0.033	0.104	0.177	75.9	7.61	
−210 + 149	1.65	8.93	0.149	<0.001	0.067	0.14	83.5	5.61	6.62
−149 + 100	1.01	4.23	0.146	<0.001	0.069	0.111	90.2	4.22	36.41
−100 + 74	0.69	1.98	0.129	<0.001	<0.001	0.079	93.5	3.63	55.05
−74 + 37	0.82	1	0.125	<0.001	0.06	0.071	94.7	3.19	
−37	1.32	1.18	0.145	<0.001	0.104	0.097	93.1	3.99	
Calculated	0.93	3.49	0.14		0.1	0.10	91.2	4.08	100

particles presented $\Psi = 0.45$ and after 90 h of pumping the value was $\Psi = 0.73$. As can be verified on the SEM images (Figs. 5 and 6), angular and elongated particles were observed in the bulk sample (Figs. 5(a) and 6 (a)), conversely, after 90-h pumping, the particles became smaller and more spherical (Figs. 5(b) and 6(b)).

3.2. Characterization of the steel coupons

The microstructure of the steel coupons after etching with Nital is shown in Fig. 7. The refined ferrite grains (grain size < 30 μm) is remarkable, as well as the presence of pearlite phase (dark region). Non-metallic inclusions uniformly distributed throughout the surface can be observed on the steel surface polished at 1 μm without etching (Fig. 8).

Fig. 8 reveals that the material has a high density of inclusions, which, according to the standard ASTM E45, can be classified as D type (globular oxides) with small diameters ($d < 3$ μm). The inclusions were examined by EDS, revealing the presence of manganese sulfide (MnS), aluminum and silicon oxides.

3.3. Corrosion results (linear polarization resistance - LPR)

The corrosion resistance of the samples in filtered iron ore slurry was analyzed for static and turbulent environments. The steel samples undergone 1-h tests and six consecutive LPR experiments were acquired,

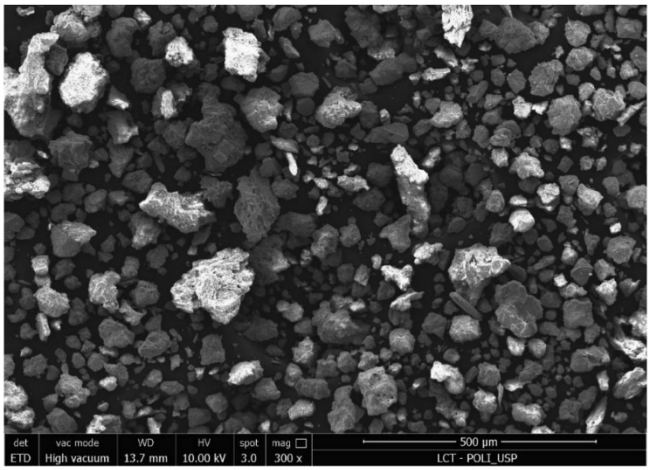

a)

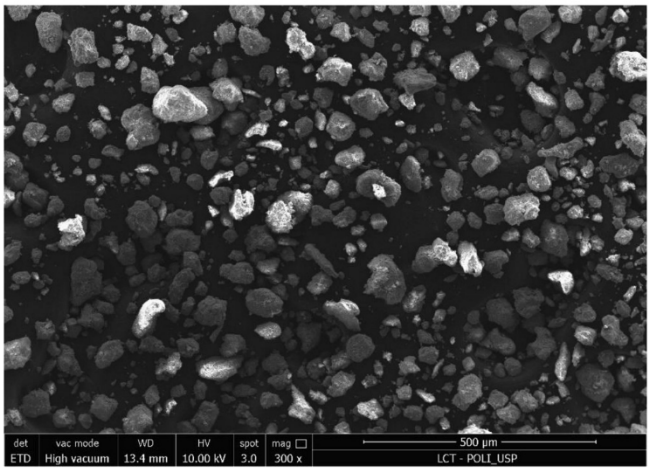

b)

Fig. 5. Secondary Electrons SEM images: a) Bulk sample. b) Sample pumped for 90 h.

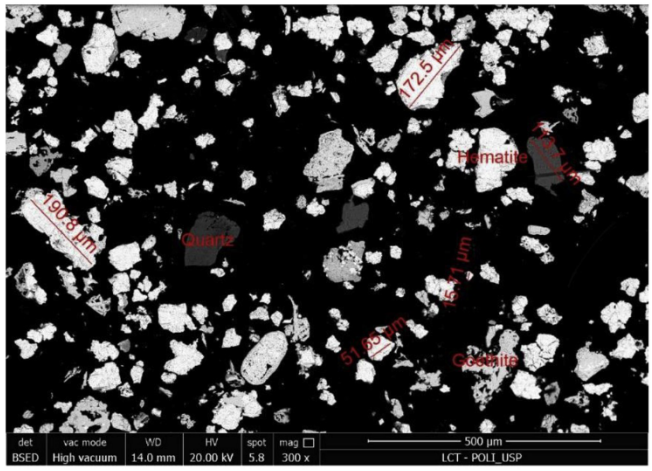

a)

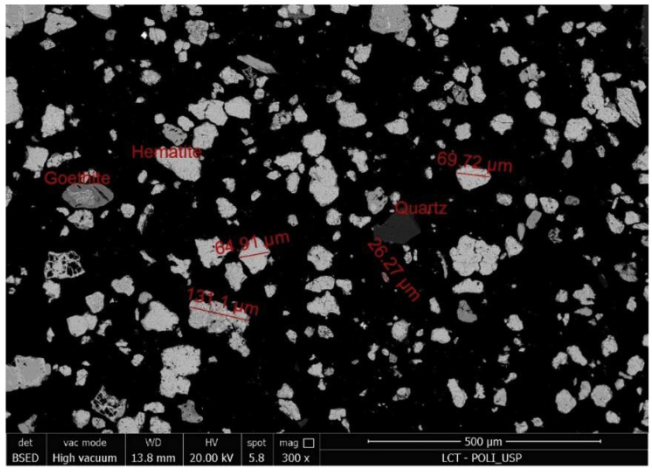

b)

Fig. 6. Backscattered electrons SEM images: a) Bulk sample. b) Sample pumped for 90 h. The mineralogical composition was confirmed by EDX.

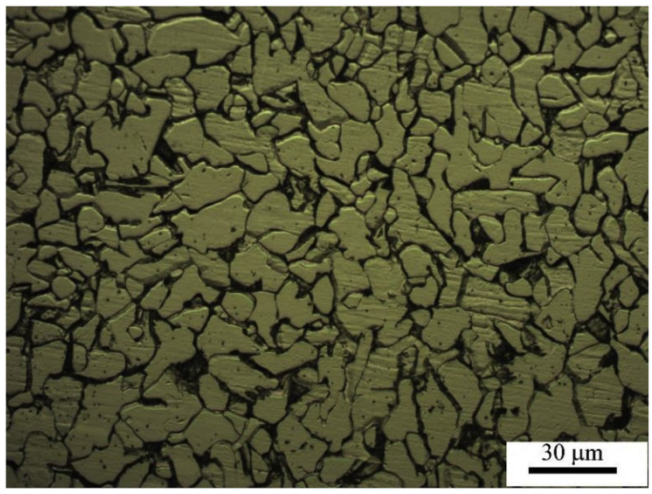

Fig. 7. Optical microscopy image of the steel coupons (2% Nital etch).

one every 10 min. Fig. 9 shows two representative LPR plots and the way to determine the Ecorr (corrosion potential, at which the current density is zero) and the Rp (polarization resistance - corresponding to the slope

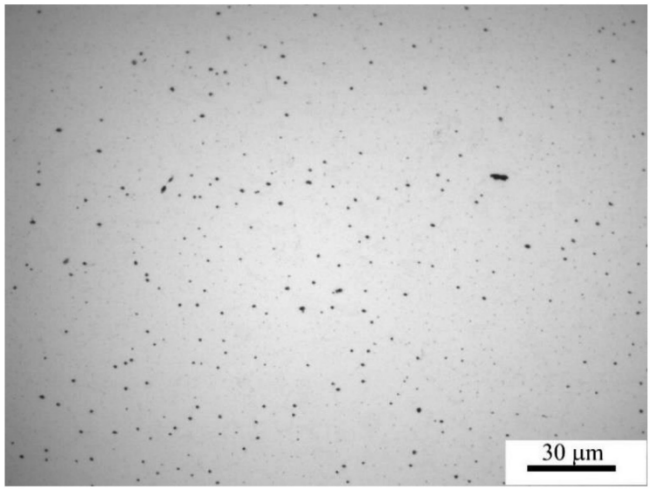

Fig. 8. Optical microscopy image of the polished surface revealing the nonmetallic inclusions.

of the plots) values; the latter was used to calculate the corrosion rate. Table 5 exhibits the Rp and Ecorr values obtained from the LPR tests and their respective average corrosion rate at each regime condition. The electrochemical tests show that the corrosion rate in the static condition was higher (0.04 mm/year) than in the turbulent condition (0.01 mm/year). Nonetheless, these values are not considered aggressive. The record of the OCP during the Rp experiments shows that it continuously decreased for the static condition, whereas it remained approximately constant for the experiments performed at turbulent regime. The differences in the behaviors may be attributed to the precipitation of corrosion products on the sample surface during the static experiment, modifying the surface conditions, thus changing the OCP.

3.4. Slurry velocities determination (pressure drop vs. slurry flow velocity)

The velocities of the wear tests were chosen according to the pressure drop curve as a function of slurry velocity (Fig. 10). From Fig. 10 analysis, it is possible to verify that the pressure drop profile presents a minimum corresponding to a critical velocity (Vc). This behavior is typical of a heterogeneous slurry flow forming a packed bed of particles in movement at the bottom of the pipe. Therefore, to guarantee a flow regime with the iron ore particles totally suspended, the velocity selected in the wear tests must be superior to Vc, *i.e.*, flow rates higher than 1.2 m/s must be selected. In Fig. 10 the two chosen velocities: 1.6 and 3.0 m/s are indicated.

3.5. Wear rate results

According to the results presented in Fig. 10, two pumping regimes were selected: 1.6 m/s and 3 m/s. In both regimes, the concentration of iron ore was 60 wt%. The wear rates of coupons exposed to the iron ore slurry after different aging times were calculated as thickness loss (mm/year) using equation (1) (Section 2.2), which is a practical way to estimate the lifetime of a pipeline by extrapolation (assuming a constant wear rate over time). Table 6 summarizes the experimental sequence

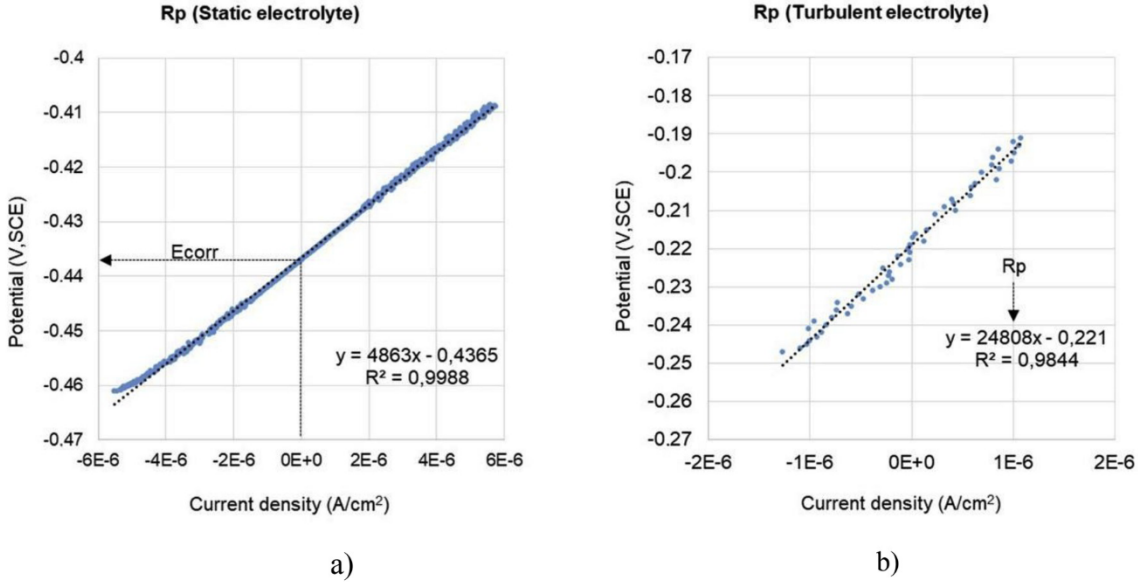

Fig. 9. Representative LPR plots. a) Static electrolyte condition showing Ecorr of −0.437 V (SCE) and a Rp slope value of 4863 Ω.cm2. b) Turbulent electrolyte condition showing an Ecorr of −0.221 V (SCE) and a Rp slope value of 24,808 Ω.cm2.

Table 5
Summary of the corrosion parameters determined from the LPR measurements.

Cond.	Test	1	2	3	4	5	6	Corrosion rate average (mm/year)
Static	Rp	5085	5534	4965	4891	4974	4912	0.04
	Ecorr	−0.390	−0.408	−0.436	−0.446	−0.471	−0.482	
Turbulent	Rp	16,842	16,780	21,730	25,580	24,808	21,780	0.01
	Ecorr	−0.231	−0.228	−0.223	−0.215	−0.221	−0.219	

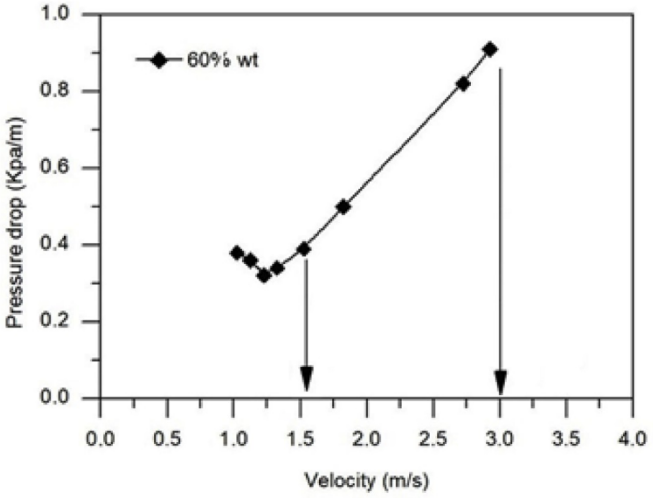

Fig. 10. Pressure drop as a function of slurry velocities. The arrows indicate the selected velocities for the slurry wear tests.

Table 6
Interval pumping times tested and their respective wear rates.

Test	Time of coupon exposure to the circulating fluid (hours)	Slurry concentration and velocity	Pumping interval examined (accumulated hours)	Wear rate calculated as thickness loss (mm/year)
First pumping session - 40 h				
Coupon 1a	8	60 wt% - 1.6 m/s	0 to 8	1.01
Coupon 2a	8		8 to 16	0.58
Coupon 3a	8		16 to 24	0.61
Coupon 4a	8		24 to 32	0.80
Coupon 5a	8		32 to 40	0.55
Coupon 6a	3		Tests sequentially	0.18
Coupon 7a	3		done with iron ore already	0.2
Coupon 8a	3		pumped for 40 h. Coupons with cathodic protection	0.16
Second pumping session - 90 h				
Coupon 1b	3	60 wt% - 3 m/s	0 to 3	0.98
Coupon 2b	6		3 to 9	0.75
Coupon 3b	10		20 to 30	0.66
Coupon 4b	10		60 to 70	0.44
Coupon 5b	3		75 to 78	0.43
Coupon 6b	10		80 to 90	0.43

and wear rate results.

Fig. 11 represents the corrosion rates, as thicknesses losses, as a function of accumulated pumping time (graphical representation of the data in Table 6). Every point denotes the wear rate of a specific pumping interval, for instance, the first black circle represents the Coupon 1b which was subjected to 3 h pumping, from the time 0 (fresh slurry) until 3 h of pumping, the second circle represents the Coupon 2b which

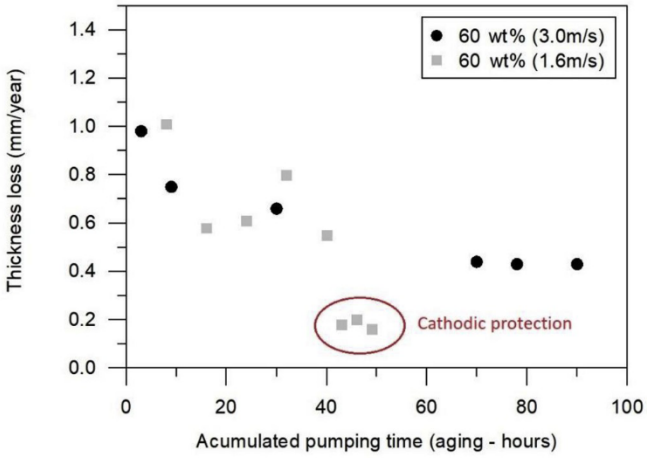

Fig. 11. Summary of thickness loss (wear rate) as a function of slurry pumping time (aging). Data calculated from the cathodic protected samples are also presented.

started the test with aged slurry (3 h of previous recirculation) and was subjected to the pumping regime for 6 h until the slurry reach 9 h of recirculation (Tables 2 and 3 summarizes the experimental sequence).

Fig. 11 shows that the erosion capacity of the iron ore slurry decreases with pumping time. However, it is clear that even after longer pumping periods, the slurry continues to be aggressive, especially in the non-protected conditions. The results allow inferring that wear rate is not influenced by the change of flow velocities in the chosen range, and that the main factor influencing the wear intensity is the recirculation slurry time, which is directly related with the morphological changes in the iron ore particles.

As explained in the experimental procedure, the experiments were performed in a large-scale loop using 1 ton of iron ore slurry as the recirculating fluid. Therefore, repetition of experiments in the same period of time is very complicated, not only due to the logistic associated with the transportation of a large amount of iron ore from the mine (640 km distance), but also due to the impossibility of keeping the iron ore particles with the same characteristics after some hours of recirculation. However, the wear rate of the experiments with cathodic protection, which were performed at close intervals, showed repeatability of the data. On the other hand, the wear rates after 60 h of pumping were similar (coupons 4b, 5b and 6b), that may indicate the stabilization of the morphology of the iron ore particles and consequently the repeatability of the system.

3.6. *Wear morphology*

The results were complemented by the wear morphology examination. The coupons were put into the pipeline always with the polished surface facing upwards (Fig. 12(a) and (b)), allowing visualizing the etching marks caused by the interaction with the ore slurry. Fig. 12(c) and (d) reveal the typical marks and morphology obtained after the wear tests, which generally presented elongated marks with evidences of corrosive attack showing discontinuities at the extremities. These discontinuities may result from the short test time, which may not have been long enough to let them merge, indicating that the corrosion process may start by a localized mechanism.

4. Discussion

This work consisted of two parts; the first one was designing a device able to determine wear directly from a large-scale flow-loop without interfering with the hydrodynamic flow; and the second was to evaluate the deterioration and to forecast the lifetime of a specific carbon steel

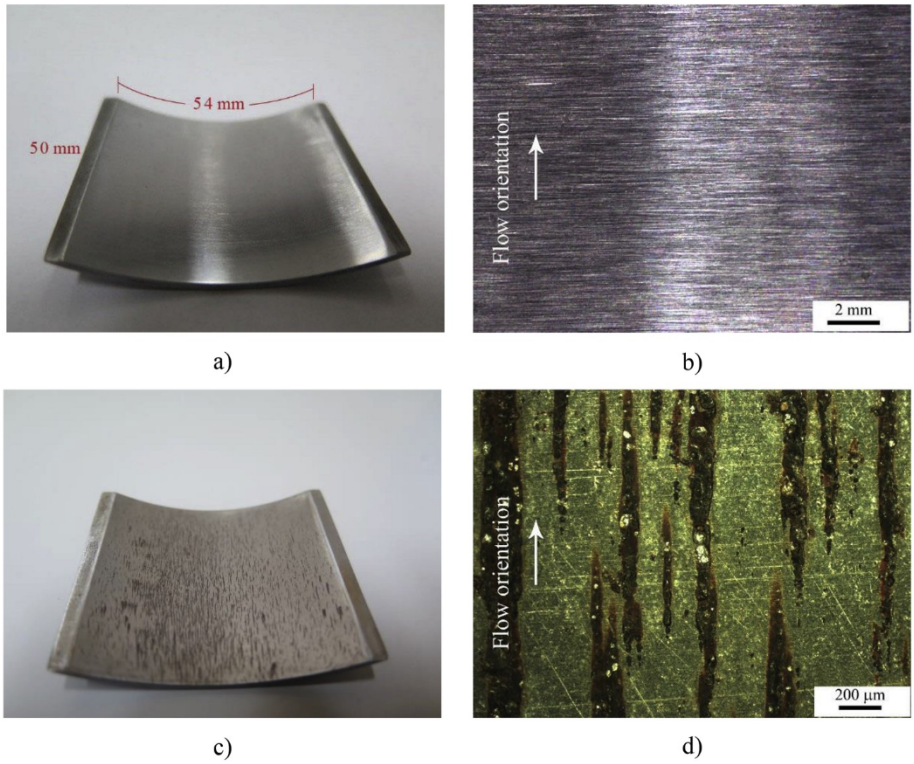

Fig. 12. Aspect of a coupon before ((a) and (b)) and after ((c) and (d)) the wear tests. The images correspond to Coupon 2b in the second pumping session - Table 6).

used in pipelines. The wear rate was determined using iron ore at 60 wt % concentration, two flow velocities and different slurry aging (pumping time), the results were correlated with the microstructure of the coupons and with the morphology of wear marks on them, as well as with the size and sphericity of the ore particles. Moreover, the evaluation of the synergism between erosion and corrosion, leading to the observed wear rates was also aimed. Therefore, pure erosion and pure corrosion damages were also evaluated.

4.1. *Pure corrosion and pure erosion damages*

Pure corrosion damages were evaluated by performing electrochemical measurements, under static and turbulent regime, with a three-electrode cell in an electrolyte consisting of the iron ore concentrate. On the other hand, to estimate pure erosion damage, the cathodic protection system already described was employed. Irrespectively to the flow regime, the results of the electrochemical tests showed a negligible corrosion rate: 0.04 mm/year in static condition and 0.01 mm/year in turbulent flow (Table 5). These values were much lower than those determined in the wear tests (Fig. 11), about at least ten times lower for the worst corrosive condition (static exposure), indicating that corrosion alone is not the main responsible for the relatively high thicknesses losses obtained when the steel coupons were exposed to the concentrated ore slurry. Indeed, after the completion of the electrochemical tests the surface of the samples became slightly reddish, but with no signs of intense corrosion, and exhibiting just a small weight loss, as documented in Table 5.

On the other hand, the experiments with the cathodically protected coupons (6a, 7a and 8a - Table 6), pure erosion tests, showed thicknesses losses of 0.18 ± 0.02 mm/year, about 3.5 times lower than the total wear (0.63 ± 0.11 mm/year - Coupons 2a, 3a, 4a, 5a - Table 6) and 4.5 times higher than the corrosion rate (0.04 mm/year – Table 5), showing that pure erosion is more detrimental to the overall behavior of the pipe than pure corrosion. This comparison is shown graphically in section 4.2 (Fig. 14).

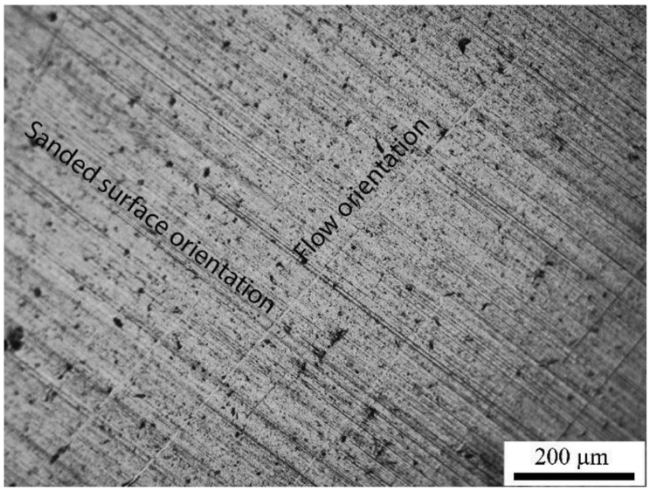

Fig. 13. Optical microscopy image of the surface of the ASTM A106 B steel tested for 3 h in iron ore slurry 60% concentration. Coupon galvanically coupled to a pure Zinc sheet.

Fig. 13 presents an optical microscopy image showing the surface morphology of a galvanically protected coupon after exposure to the iron ore slurry. It shows that the ore particles scratched the surface in the flow orientation direction, and reveals that erosion starts as scratches that must be mainly created by the hardest particles of the slurry - quartz between 6.5 and 7 in Mohs scale and hematite approximately 5.5 Mohs scale, both harder than the coupon with 84 Rockwell B (a hardness equivalent to 3 to 4 Mohs) [46]. Fig. 13 also indicates that the particles slide on the surface, squeezing the metal ahead and to the sides to form ridges which occur due to the low impact angle and low particle velocity, an erosion mechanism known as ploughing. Differently from cutting mechanism, ploughing does not remove material from the

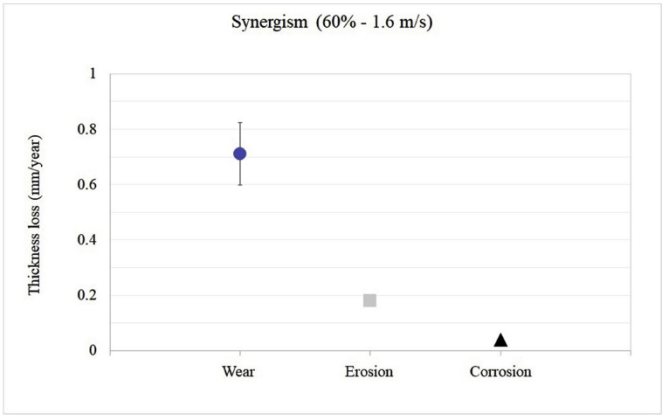

Fig. 14. Mean thickness losses by wear, pure erosion and pure corrosion.

surface, just shifts it to the side of the erosion groove [47].

4.2. Erosion-corrosion synergism

Fig. 14 displays the comparison between the corrosion rates, as thicknesses losses (mm/year), for the pure corrosion (static experiments) and erosion tests (coupons 6a, 7a and 8a-Table 6), and the mean wear rate determined from the tests performed with coupons 2a, 3a, 4a, 5a and 6a (Table 6). After these pumping time the wear rate seems to have achieved a steady state, therefore a valuable comparative basis can be established. The plot clearly shows synergism as the total wear rate is higher than the sum of the contributions of pure erosion and pure corrosion individually.

Fig. 15 displays a 3D profilometry image of a sample exposed during 3 h to the iron ore slurry just before the acquisition of the data for the cathodically protected samples. It reveals that in the absence of cathodic protection the wear marks initially grow as microcraters aligned in the flow direction. As previously discussed, erosion takes place by a ploughing mechanism, in the case of wear damage (erosion + corrosion), the continuous exposure of fresh metal surface to the aggressive environment due to the impact of the hardest particles enhances the electrochemical activity of the flowing slurry, increasing the corrosion rate and creating the elongated morphology shown in the OM image of Fig. 12(d), suggesting merging of neighboring craters. Comparing the grain sizes of the steel microstructure (Fig. 7), with the dimensions of the microcraters in Fig. 15, a similar size (around 30 μm) can be observed. This suggests that a particular type of steel grain, possibly grains with a preferential crystallographic orientation, is more susceptible to electrochemical activation, originating the microcraters. This statement is supported by the literature since several researchers have reported that crystallographic orientation affects the friction coefficient and the wear micro-mechanisms [48–55]. Additionally, the studied steel was observed to have a considerable quantity of nonmetallic inclusions (Fig. 8), which also play a key role as preferential sites for corrosion initiation [56–59].

4.3. Relationship between the wear rate, ore particle size and sphericity

Fig. 16 presents the variation of the particle size and sphericity of the iron ore slurry as a function of the pumping time (aging). It shows that the iron particles sizes (% particles > 75 μm size fraction) changes from 44% in the bulk material to 24% in the material pumped for 90 h. Regarding sphericity, the bulk material presented $\Psi = 0.45$, whereas after 90 h of pumping, the tests indicate $\Psi = 0.73$ ($\Psi = 1$ represents complete sphericity). A comparison with the data presented in Fig. 11 shows that the wear rate tends to decrease as the ore particles sizes decrease and the sphericity increases, which is in accordance with the literature [60]. Indeed, the effect of abrasive grains sizes on the wear rate is a theme that has received considerable attention in the literature [61–72]. In a broad sense, the lower the abrasive grain size, the smaller the wear rate will be, either for two bodies or three bodies abrasion as well as for erosion [73–75]. Particularly, the decrease of the abrasive size due to abrasive fracture during wear tests was conclusively demonstrated by Bozzi and De Mello [76].

4.4. Pipeline lifetime forecast

The pumping system used is a recirculation pilot loop, therefore, by

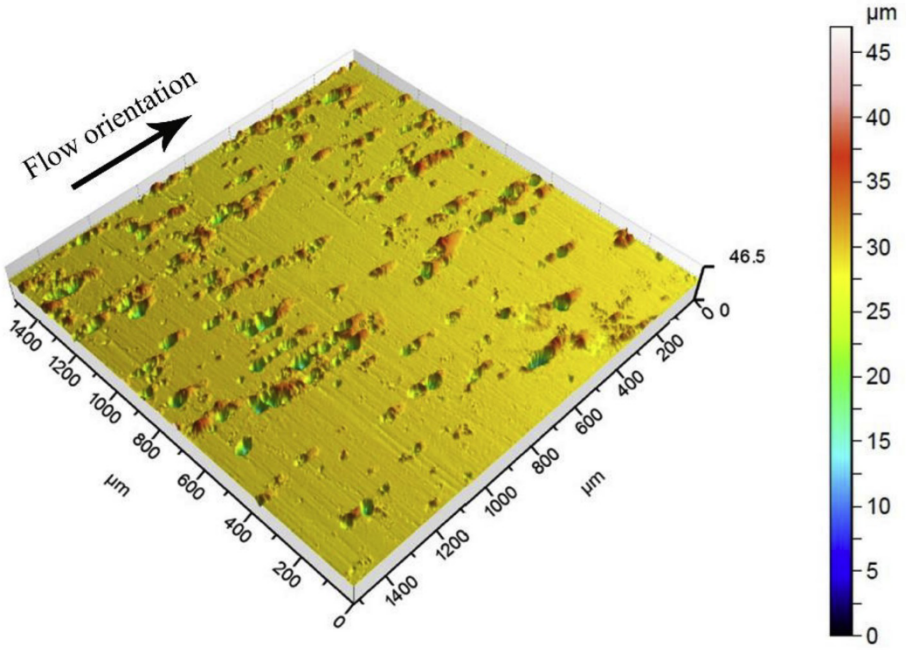

Fig. 15. 3D optical profilometry image of the coupon surface after 3-h exposure to iron ore slurry concentrated at 60 wt% and flow velocity 1.6 m/s. Cathodic protection was not employed.

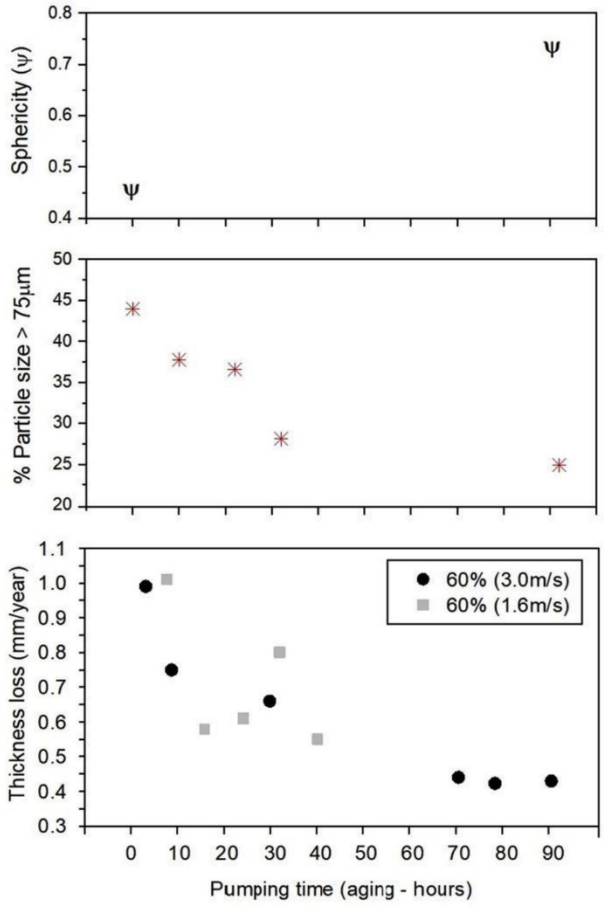

Fig. 16. Sphericity, particle size and thickness loss (wear rate) changes and as a function of slurry aging.

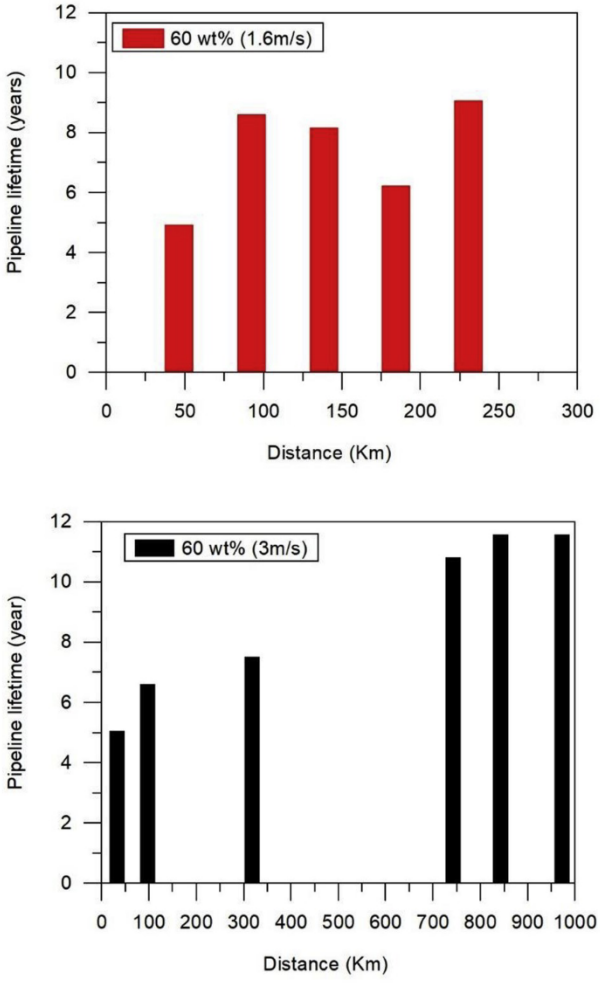

Fig. 17. Simulation of failure by wear (pipeline lifetime) of a 5 mm thickness pipeline as a function of distance travelled by the iron ore slurry. a) 1.6 m/s and b) 3 m/s.

knowing the accumulated pumping time (fourth column of Table 6) and the slurry velocities (3 m/s or 1.6 m/s), it is possible to estimate the wear rate simulating the behavior of a long-distance pipeline, enabling to evaluate the wear potential of the aged slurry at a given distance. If the operating parameters of the slurry pipeline are kept constant (temperature, initial iron ore slurry characteristics, pressure drop, velocity, concentration, and pH), at a given distance, the wear rate can be supposed to be constant over time, allowing estimating (by extrapolation) the decrease of the pipeline thickness as a function of the distance covered by the iron ore slurry.

Fig. 17 shows the estimated time required for a 5-mm thickness reduction to occur at different distances along the pipeline length (data calculated from wear rate results - Fig. 11 and Table 6). It indicates that the iron ore slurry is very aggressive regardless to the travelled distance. Analyzing the results for the iron ore slurry concentrated at 1.6 m/s, for the first covered distance, 46 km (achieved after 8 h pumping), the time necessary for the thickness to be reduced by 5 mm is less than 5 years. However, when the pumping time reaches 40 h, equivalent to a travelled distance of 230 km (representing a long-distance pipeline), the necessary time to reach the same thickness reduction is approximately 9 years, corresponding to an increase of 80% in the estimated lifetime. For the velocity of 3 m/s, the results were relatively similar, and for the tests corresponding to travelled distances of 97 km (9 h) and 324 km (30 h), the 5-mm thickness reduction takes place after 6.6 and 7.6 years, respectively. Conversely, considering only the worst scenario depicted by the corrosion tests (Rp measurements under static conditions (0.04 mm/year) and considering a uniform corrosion rate, the time for a 5 mm thickness loss would be more than 100 years, indicating that, from the sole corrosion point of view the tested steel is quite resistant (note that this failure time is an overestimation as neither localized corrosion nor the pumping pressure effects were taken into account). These results highlight the importance of the particle size and sphericity in the wear capability of the iron ore slurry. It is important to emphasize that wear rates were calculated considering the total exposed area of each coupon (27 cm^2) and not on the wear marked areas (Fig. 12(d)). As the latter areas are smaller than the total area of the coupons, the pipeline lifetime is expected to be lower than that estimated.

The development of this investigation confirmed that the specific literature is quite restricted, as pipelines failures cases are not commonly shared by the mining industry. From the databases consulted, only two published works about wear and corrosion rates in pipelines caused by iron ore slurry transportation were found, one published in 1974 [35] and other in 1979 [77]. The first investigation [35] determined the corrosion rate caused by iron ore slurry (SG 5.16, Fe, 66.28%, SiO2, 2.29%, Mn, 1.71%, balance Oxygen, mean size 0.21 mm, Cmax 24%) and iron concentrate slurry (70% passing 200 mesh, mean size < 0.04 mm, Cmax 30%.) using a closed loop (50 mm diameter pipeline) with an electrochemical arrangement coupled to a potentiostat equipment. The material analyzed was ASTM A53 carbon steel (Nominal composition - wt%: C, 0.1, Mn, 0.5, Cu, 0.2, Ni, 0.12, P, 0.01, S, 0.03) and the range of velocities applied were 1.5 m/s to 3.1 m/s. Although the materials, velocities and concentrations analyzed were relatively similar to those used in the present investigation, the results are not in accordance. The authors [35] reported corrosion rates from 13 mm/year to 25 mm/year

while we measured much lower wear rates (1.01 mm/year in the worst condition considering wear (erosion and corrosion synergism)). These differences could be attributed to several factors, for example, the hardness of the ASTM A106 steel used in this work is 84 Rockwell B while the ASTM A53 steel used by the other authors [35] in 1974 had 70 Rockwell B hardness. The ore concentrated grain sizes were similar in both works, but the iron ore used in Ref. [35] was larger (mean size 0.21 mm), whereas in the present investigation 95% of the pellet feed ore was smaller than 0.21 mm (Figs. 4 and 5). Nevertheless, considering that the wear rates determined in both investigations are notably different, and that the weight loss technique is a direct measurement (more realistic), possible failures in data acquisition by the electrochemical technique can be supposed, such as the IR drop caused by the turbulent regime and/or problems related with the design of the electrochemical cell. Five years later, the same author [77] published an investigation about the use of corrosion inhibitors in iron ore slurry (grain size 93.5 < 0.04 mm; 60 wt% concentration). In that case, the loop, steel samples (ASTM A53), slurry velocity (2.1 m/s) and the electrochemical technique used were the same used in 1974 [35], but this time the results were similar to the results presented herein (corrosion rate measurements oscillating between 0.16 mm/year and 0.46 mm/year) which are in accordance with the present work (Table 6).

Finally, it is important to clarify that, at the current stage, this research has contributed to understanding the wear mechanism occurring in iron ore slurry transportation, but cannot be used as a base for pipelines design as no effective estimation of localized corrosion damage was performed. This is a subject of an ongoing research.

5. Conclusions

The wear caused by iron ore slurry transportation was evaluated by means of a new coupon system facility that allowed studying the tribological interactions between the flow slurry particles and the pipeline surface in a closed loop. From this study, the following conclusions can be drawn:

- The results from the pilot-scale-loop conjugated to the wear coupon system were satisfactory and allowed determining the wear rate as a function of pumping time and slurry flow velocity. With respect to flow velocity, no significant differences were noted in the wear when applying 3 m/s or 1.6 m/s.
- As expected, the wear rate decreases with the iron ore slurry aging (due to rounding and decreasing of the particles sizes). Nevertheless, the results revealed that even after long-time pumping (equivalent to long distance pipelines) the iron ore slurry continues to be highly aggressive to the ASTM steel.
- Pure corrosion effects, evaluated by means of electrochemical tests performed in the absence of abrasive particles, and pure erosion effects, assessed by means of a cathodic protection system, revealed that the damages caused by these two types of mechanism were much lower than the registered wear. This indicates an important synergistic effect between erosion and corrosion during wear, likely caused by the constant exposure of fresh metal to the aggressive electrolyte, enhancing the electrochemical activity and leading to the merging of aligned wear microcraters, as revealed by profilometry observations.

Declaration of competing interest

The authors declare that they have no known competing financial interests or personal relationships that could have appeared to influence the work reported in this paper.

Acknowledgments

The authors would like to acknowledge the financial support of ITV MI, CAPES, FAPESP and CNPq. VALE S.A. is fully acknowledge for providing the iron ore concentrate.

References

[1] USGS. U.S. Geological Survey, Mineral Commodity Summaries, January, 2018, pp. 88–89. Available in: https://minerals.usgs.gov/minerals/pubs/commodity/iron_ore/mcs-2018-feore.pdf.
[2] T.C. Souza Pinto, P.T. Slatter, P.H. Matai, L.S. Leal Filho, The influence of particle shape on stratification in pipe flow, Powder Technol. 302 (2016) 75–80.
[3] R. Tarodiya, B.K. Gandhi, Hydraulic performance and erosive wear of centrifugal pumps – a review, Powder Technol. 305 (2017) 27–38, https://doi.org/10.1016/j.ptech.2016.09.048.
[4] Mtpa, Ministério dos Transportes, Portos e Aviação Civi. Corredores logísticos extrategicos. Vol II (complexo de minério de ferro), 2018, p. 68.
[5] The Hindu, Online edition of India's national newspaper. Activists intensify campaign against mining in Kudremukh (Sunday, August 19, 2001). By Shivaraja B.Nanjhappa, Available in: https://www.thehindu.com/thehindu/2001/08/19/stories/0419210o.htm.
[6] The Times of India News Service, Kudremukh loses Rs 22.5 due to slurry leak, Available in: http://www.indiatogether.org/campaigns/kudremukh/kudTOI2507a.html. Accesed (17/11/18.
[7] Pipeline Information Center, Available in: https://brasil.angloamerican.com/vazamento-do-mineroduto/pipeline-information-center?sc_lang=pt-PT. (Accessed 15 November 2018).
[8] S. Bhattacharyya, F.C. Bock, Abrasive wear of engineering materials by mineral and industrial wastes, Wear 46 (1978) 1–18.
[9] E. Rabinowicz, Friction and Wear of Materials, John Wiley & Sons, Inc., New York, 1984.
[10] National Research Council Canada, A Strategy for Tribology in Canada: Enhancing Reliability and Efficiency through the Reduction of Wear and Friction, Technical report, 1986.
[11] Kenneth Holmberg, Päivi Kivikytö-Reponen, Pirita Härkisaari, Kati Valtonen, Erdemir Ali, Global energy consumption due to friction and wear in the mining industry, Tribol. Int. 115 (2017) 116–139, https://doi.org/10.1016/j.triboint.2017.05.010.
[12] Brent W. Madsen, Measurement of erosion-corrosion synergism with a slurry wear test apparatus, Wear 123 (1988) 127–142.
[13] Yugui Zheng, Zhiming Yao, Xiangyun Wei, Wei Ke, The synergistic effect between erosion and corrosion in acidic slurry medium, Wear 186 (2007) 555–561, https://doi.org/10.1016/0043-1648 (95)07132-6.
[14] S.S. Rajahram, T.J. Harvey, R.J.K. Wood, Erosion–corrosion resistance of engineering materials in various test conditions, Wear 267 (2009) 244–254.
[15] T.J. Harvey, J.A. Wharton, R.J.K. Wood, Development of synergy model for erosion-corrosion of carbon steel in a slurry pot, Tribol. Mater. Surface Interfac. 1 (2007) 33–47.
[16] H.M. Clark, K.K. Wong, Impact angle, particle energy and mass loss in erosion by dilute slurries, Wear 186–187 (1995) 454–464.
[17] H.M. Clark, Particle velocity and size effects in laboratory slurry erosion measurements OR... Do you know what your particles are doing? Tribol. Int. (2002) 617–624.
[18] H.M. Clark, R.B. Hartwich, A re-examination of the 'particle size' effect in slurry erosion, Wear 248 (2001) 147–161.
[19] H.M. Clark, On the impact rate and impact energy of particles in a slurry pot erosion tester, Wear 147 (1991) 165–183.
[20] H.M. Clark, Specimen diameter, impact velocity, erosion rate and particle density in a slurry pot erosion tester, Wear 162–164 (1993) 669–678.
[21] J. Feyerl, G. Mori, S. Holzleitner, J. Haberl, M. Oberndorfer, W. Havlik, C. Monetti, Erosion-corrosion of carbon steels in a laboratory: three-phase flow, Corrosion NACE 64 (2008) 175–186.
[22] Ma Liang, Cheng Huang, Yongsong Xie, Jiaren Jiang, Kidus Yoseph Tufa, Rob Hui, Zhong-Sheng Liu, Modeling of erodent particle trajectories in slurry flow, Wear 334 (2015) 49–55.
[23] J.B. Zu, I.M. Hutchings, G.T. Burstein, Design of a slurry erosion test rig, Wear 140 (1990) 331–344.
[24] R.J.K. Wood, J.A. Wharton, A.J. Speyer, K.S. Tan, Investigation of erosion–corrosion processes using electrochemical noise measurement, Tribol. Int. 35 (2002) 631–641.
[25] A.J. Speyer, Wear Corrosion Sensing in Flowing Seawater, Ph.D. Thesis, University of Southampton, 2002.
[26] K.S. Tan, J.A. Wharton, R.J.K. Wood, Solid particle erosion–corrosion behaviour of a novel HVOF nickel aluminium bronze coating for marine applications—correlation between mass loss and electrochemical measurements, Wear 258 (2005) 629–640.
[27] A. Neville, T. Hodgkiess, J.T. Dallas, A study of the erosion–corrosion behavior of engineering steels for marine pumping applications, Wear 186–187 (1995) 497–507.
[28] H.M. Clark, H.M. Hawthorne, Y. Xie, Wear rates and specific energies of some ceramic, cermet and metallic coatings determined in the Coriolis erosion tester, Wear 233–235 (1999) 319–327.
[29] H.M. Clark, J. Tuzson, K.K. Wong, Measurements of specific energies for erosive wear using a Coriolis erosion tester, Wear 241 (2000) 1–9.
[30] Y. Xie, H.M. Clark, H.M. Hawthorne, Modelling slurry particle dynamics in the coriolis erosion tester, Wear 225–229 (1999) 405–416.

[31] B.R. Tian, Y.F. Cheng, Electrochemical corrosion behavior of X-65 steel in the simulated oil sand slurry. I: effects of hydrodynamic condition, Corrosion Sci. 50 (2008) 773–779.
[32] M.M. Stack, J.S. James, Q. Lu, Erosion–corrosion of chromium steel in a rotating cylinder electrode system: some comments on particle size effects, Wear 256 (2004) 557–564.
[33] M.M. Stack, H.W. Wang, Simplifying the erosion–corrosion mechanism map for erosion of thin coatings in aqueous slurries, Wear 233–235 (1999) 542–551.
[34] M.M. Stack, H.W. Wang, W.D. Munz, Some thoughts on the construction of erosion–corrosion maps for PVD coated steels in aqueous environment, Surf. Coating. Technol. 113 (1999) 52–62.
[35] J. Postlewaite, E.B. Tinker, M.W. Hawrylak, Erosion- corrosion in slurry pipelines, Corrosion NACE 30 (1974) 285–290.
[36] U. Lotz, J. Postlethwaite, Erosion-corrosion in disturbed two phase liquid/particle flow, Corrosion Sci. 30 (1990) 95–106.
[37] W. Blatt, T. Kohley, U. Lotz, E. Heitz, The influence of hydrodynamics on erosion-corrosion in two-phase liquid-particle flow, Corrosion NACE (45) (1989) 793–804.
[38] R.J.K. Wood, T.F. Jones, J. Ganeshalingam, N.J. Miles, Comparison of predicted and experimental erosion estimates in slurry ducts, Wear 256 (2004) 937–947.
[39] R.J.K. Wood, T.F. Jones, Investigations of sand-water induced erosive wear of AISI 304L stainless steel pipes by pilot-scale and laboratory-scale testing, Wear 255 (2003) 206–218.
[40] K.C. Wilson, G.R. Addie, R. Clift, Slurry Transport Using Centrifugal Pumps, Elsevier Science, 1992.
[41] C.A. Shook, D.B. Haas, W.H.W. Husband, M. Small, Relative wear rate determinations for slurry pipelines, J. Pipelines 1 (1981) 273–280.
[42] R. Cooke, G. Graeme Johnson, P. Goosen, Laboratory Apparatus for Evaluating Slurry Pipeline Wear. South Africa Institute of Tribology (SAIT) - Seminar Economics of Wear Materials, 13 March 2000.
[43] R.C.N. Liberto, Corrosão-erosão da liga Cu10Ni-3Al-1, 3Fe em presença de íons cloreto, sulfeto e sulfato, PhD. Thesis, Escola Politécnica da Universidade de São Paulo, https://doi:10.11606/T.3.2010.tde-11082010-140806, 2010.
[44] F. Huet, R.P. Nogueira, H. Takenouti, Aqueous corrosion reaction mechanisms, corrosion: fundamentals, testing, and protection, in: ASM Handbook, 13A, ASM International, 2003, pp. 52–60.
[45] T.C. Souza Pinto, O.A. Lima, L.S. Leal Filho, Sphericity of apatite particles determined by gas permeability through packed beds, Miner. Metall. Process. 26 (2009) 105–108.
[46] Asm International, ASM Handbook, vol. 18, ASM International, Materials Park, OH, 1992, p. 346.
[47] Vahid Javaheri, David Porter, Veli-Tapani Kuokkala, Slurry erosion of steel – review of tests, mechanisms and materials, Wear 408–409 (2018) 248–273, https://doi.org/10.1016/j.wear.2018.05.010.
[48] Xianghui Meng, Congcong Fang, Ke Niu, Tribological behavior anisotropy in sliding interaction of asperities on single-crystal α-iron: a quasi-continuum study, Tribol. Int. 118 (2018) 347–359.
[49] P.C. Machado, J.I. Pereira, J.J. Penagos, T. Yonamine, A. Sinatora, The effect of in-service work hardening and crystallographic orientation on the micro-scratch wear of Hadfield steel, Wear 376–377 (2017) 1064–1073.
[50] M. Walter, S. Weber, J. Boes, G. Egels, W. Theisen, Mechanisms of severe sliding abrasion of single phase steels at elevated temperatures: influence of lattice structure and microstructural parameters, Wear 376–377 (2017) 468–483.
[51] K. Geenen, S. Huth, W. Theisen, Influence of crystallographic orientation on cavitation erosion resistance of high interstitial CrMnCN austenitic stainless steels, Tribol. Int. 95 (2016) 66–75.
[52] O.J. McCarthy, J.P. McGarry, S.B. Leen, The effect of grain orientation on fretting fatigue plasticity and life prediction, Tribol. Int. 76 (2014) 100–115.
[53] M. Sharif Uddin, K.H.W. Seah, X.P. Li, M. Rahman, K. Liu, Effect of crystallographic orientation on wear of diamond tools for nano-scale ductile cutting of silicone, Wear 257 (2004) 751–759.
[54] J.F. dos Santos, C.M. Garzón, A.P. Tschiptschin, Improvement of the cavitation erosion resistance of an AISI 304L austenitic stainless steel by high temperature gas nitriding, Mater. Sci. Eng. 382 (2004) 378–386, https://doi.org/10.1016/j.msea.2004.05.003.
[55] D.H. Mesa Grajales, C.M. Garzón Ospina, A.P. Tschiptschin, Mesoscale plasticity anisotropy at the earliest stages of cavitation-erosion damage of a high nitrogen austenitic stainless steel, Wear 267 (2009) 99–103, https://doi.org/10.1016/j.wear.2008.12.079.
[56] Tatyana V. Shibaeva, Veronika K. Laurinavichyute, Galina A. Tsirlina, Alexander M. Arsenkin, Konstantin V. Grigorovich, The effect of microstructure and non-metallic inclusions on corrosion behavior of low carbon steel in chloride containing solutions, Corrosion Sci. 80 (2014) 299–308.
[57] I.I. Reformatskaya, I.G. Rodionova, YuA. Beilin, L.A. Nisel'son, A.N. Podobaev, The effect of nonmetal inclusions and microstructure on local corrosion o carbon and low-alloyed steels, Protect. Met. 40 (2004) 447–452.
[58] I.I. Reformatskaya, A.N. Podobaev, G.M. Florianovich, I.I. Ashcheulova, Evaluation of the corrosion resistance of low-carbon pipe steels under conditions of hot-water supply, Protect. Met. 35 (1999) 4–9.
[59] YaM. Kolotyrkin, L.I. Freiman, The role of nonmetallic inclusions in corrosion processes, in: Achievements of Science and Technology, Series Corrosion and Corrosion Control, vol. 6, VINITI, Moscow, 1978, pp. 5–52.
[60] G. B Stachowiak, G. W Stachowiak, The effects of particle characteristics on three-body abrasive wear, Wear 249 (2001) 201–207, https://doi.org/10.1016/S0043-1648(01)00557-9.
[61] W.E. Avient, J. Goddard, H. Wilman, An experimental study of friction and wear during abrasion of metals, Proc. Roy. Soc. Lond. Math. Phys. Sci. 258 (1960) 159–180.
[62] E. Rabinowicz, L.A. Dunn, P.G. Russell, A study of abrasive wear under three-body conditions, Wear 4 (1961) 345–355, https://doi.org/10.1016/0043-1648(61)90002-3.
[63] J. Goddard, H. Wilman, A theory of friction and wear during the abrasion of metals, Wear 5 (1962) 114–135, https://doi.org/10.1016/0043-1648(62)90235-1.
[64] E. Rabinowicz, A. Mutis, Effect of abrasive particle size on wear, Wear 8 (1965) 381–390, https://doi.org/10.1016/0043-1648(65)90169-9.
[65] G.K. Nathan, W.J.D. Jones, The empirical relationship between abrasive wear and the applied conditions, Wear 9 (1966) 300–309, https://doi.org/10.1016/0043-1648(66)90004-4.
[66] J. Larsen-Badse, Influence of grit diameter and specimen size on wear during sliding abrasion, Wear 12 (1968) 35–53, https://doi.org/10.1016/0043-1648(68)90574-7.
[67] J. Larsen-Badse, Abrasion resistance of some S.A.P.-type alloys at room temperature, Wear 12 (1968) 357–368, https://doi.org/10.1016/0043-164868)90538-3.
[68] L.E. Samuels, Metallographic Polishing by Mechanical Methods, second ed., Sir Isaac Pitman & Sons Ltd. Melbourne & London, 1971.
[69] S.W. Date, S. Malkin, Effects of grit size on abrasion with coated abrasives, Wear 40 (1976) 223–235, https://doi.org/10.1016/0043-1648(76)90100-9.
[70] H. Sin, N. Saka, N.P. Suh, Abrasive wear mechanisms and the grit size effect, Wear 55 (1979) 163–190, https://doi.org/10.1016/0043-1648(79)90188-1.
[71] J.J. Coronado, A. Sinatora, Effect of abrasive size on wear of metallic materials and its relationship with microchips morphology and wear micromechanisms: Part 1, Wear 271 (9–10) (2011) 1794–1803, https://doi.org/10.1016/j.wear.2011.01.078.
[72] J.J. Coronado, A. Sinatora, Effect of abrasive size on wear of metallic materials and its relationship with microchips morphology and wear micromechanisms: Part 2, Wear 271 (2011) 1804–1812, https://doi.org/10.1016/j.wear.2011.05.036.
[73] Ambrish Misra, Iain Finnie, On the size effect in abrasive and erosive wear, Wear 65 (1981) 359–373, https://doi.org/10.1016/0043-1648(81)90062-4.
[74] Ambrish Misra, Iain Finnie, Correlations between two-body and three-body abrasion and erosion of metals, Wear 68 (1981) 33–39, https://doi.org/10.1016/0043-1648(81)90017-X.
[75] Ambrish Misra, Iain Finnie, Some observations on two-body abrasive wear, Wear 68 (1981) 41–56, https://doi.org/10.1016/0043-1648(81)90018-1.
[76] Antônio César Bozzi, José Daniel Biasoli de Mello, Wear resistance and wear mechanisms of WC–12%Co thermal sprayed coatings in three-body abrasion, Wear 233–235 (1999) 575–587, https://doi.org/10.1016/S0043-1648(99)00206-9. ISSN 0043-1648.
[77] J. Postlethwaite, Electrochemical studies of inhibitors in aqueous slurries of sand, iron ore and coal, Corrosion-NACE 35 (1979) 475–480.